Performances Comparison of Permanent Magnet Brushless DC and Doubly Salient Reluctance Motors for an Urban Electric Vehicle

Bernard Multon, Emmanuel Hoang, François Camus

Performance comparison of permanent-magnet brushless DC and doubly-salient variable-reluctance motors for an urban electric vehicle

B. Multon, E. Hoang and F. Camus

In this paper, a dimensional parameter analysis of the average torque and copper losses for two synchronous brushless motors is carried out. A permanent-magnet brushless DC motor (PMBLDCM) with surface-mounted magnet rotor and trapezoidal e.m.f.-waveform, supplied by quasi-square currents, and a doubly-salient variable-reluctance motor (DSVRM) fed by quasi-square currents, at low speed, and by full-wave square voltages, at high speed, are compared. Both motors have three phases; the DSVRM possesses a 6/4 structure and the PMBLDC has two pairs of poles and only one slot per pole and per phase. The comparison shows that the performances of DSRVM are close to those of high-energy PMBLDCM thanks to the former's short winding-ends and good slot-filling factor, insofar as the airgap is sufficiently small, in accordance with the requirements of electric vehicles.

1. Introduction

The motor choice for an electric vehicle is a dificulty task. A great number of parameters have to be taken into account. The electric motor must be low-cost, light and highly efficient. With a fixed gear-ratio, the motor must be able to operate on a wide maximum-power speed range. Whatever is the electromagnetic motor, its torque determines the motor size. Copper losses are highly dependent on average torque; increasing the number of poles allows to grow torque mass ratio, but frequency and magnetic losses will also increase. To obtain a high power mass ratio, high-speed operation is required [12]. The determination of the number of poles and gear-ratio is very important if a satisfactory compromise between power mass ratio and efficiency of gear motor set must be achieved. However, there is an economical optimum in the gear-ratio choice. Moreover, cost and acoustic noise impose a maximum speed of about 10 000 rpm.

In this paper an urban vehicle developing 27 kW mechanical power over a 2 500 to 10 000 rpm speed range is chosen as an example. A single-motor solution is adopted. For a 10 000 rpm maximum motor speed a 10:1 gear-ratio and a 100 Nm maximum average torque are available.

Several types of electromagnetic motors have been considered for driving electric vehicles, such as DC, induction, permanent-magnet synchronous and variable-reluctance motors [22]. Chopper-fed DC motors are known to offer, for the moment, the best performances vs. cost compromise, but their limitations in terms of maintenance and power mass ratio have led us to study brushless motors.

Permanent-magnet brushless DC motors (PMBL DCM) with high-energy magnets are known to have the best efficiency, but their cost is higher than that of their competitors [1]. *Doubly-salient variable-reluctance motors* (DSVRM), also called *switched reluctance motors*, certainly are the most economical and robust ones, but their performances have to be compared with those of other motors [4, 5, 6]. It is proposed a parametric comparison between DSVRM and PMBLDCM based on the electromechanical conversion. Surface-mounted magnet motors are considered as PMBLDCM, their performance being slightly superior to those of inset-magnet [7] and interior-magnet [9] motors. Both DSVRM and PMBL DCM are simple and suitable for mass production, but require self-commutation by means of either direct or indirect position sensors [2].

In the following, operating principles and distinctive features of these two types of motors are outlined.

In DSVRM, particularly those with wound "big teeth" [1, 4, 5, 6], one can consider that the stator consists of a series of p electromagnets per phase (in a 6/4 structure, $p = 2$). If q is the number of phases, the number of stator poles (or teeth) results $N_s = pq$.

When excited, the p electromagnets of each phase attract p rotor teeth from their total number N_r . As the forces are not dependent on the curent sense, a DSVRM can be fed from a specific converter consisting of a q asymmetrical half-bridges. This particularity ensures increased running safety in comparison with classical three-phase bridge-type converters.

PMBLDCM are well known [1]; their stator consists of N_s slots containing windings, which are arranged in q phases (with p pairs of poles) and in m_e slots per pole and per phase to obtain the required m.m.f. waveform. The rotor consists of $2p$ surface-mounted, radially and alternately magnetized permanent-magnets. It is considered here a three-phase motor fed by rectangular, bipolar current-waveform. If the e.m.f.s are trapezoidal, the electromagnetic torque is approximately constant and proportional to the phase-current amplitude.

The structures of both brushless motors are shown in Fig. 1. The DSVRM has 6/4 structure, including 6 stator poles with concentrated windings and 4 poles (or teeth) in the rotor. Both rotor and stator magnetic circuits are laminated. The stator has three phases consisting of two diametrically-opposed wound poles.

In its turn, the three-phase PMBLDC shown in Fig. 1 consists of 4 surface-mounted permanent magnets ($p = 2$) glued on a ferromagnetic yoke (either laminated or massive) and mechanically held by a sleeve. The windings are placed in slots with only one slot per pole and per phase ($m_e = 1$).

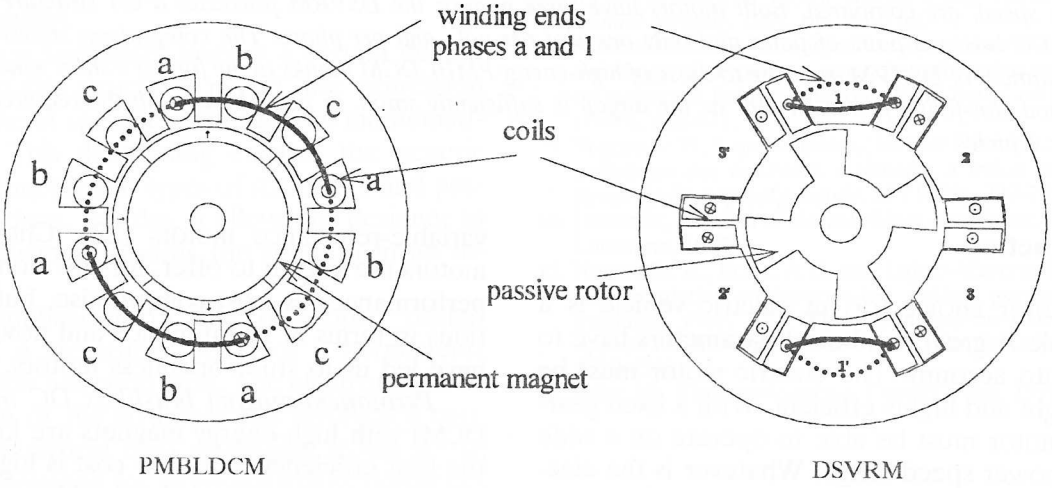

Fig. 1. Structures of compared motors.

Fig. 2 shows the electronic converter structures and corresponding ideal supply waveforms for both motors. The reference for self-commutation is the phase inductance for DSRVM and the e.m.f. for PMBLDCM, respectively. Below the base speed, the DSRVM phases are fed by current-controlled waveforms so as to obtain constant torque operation. [18, 25]. Above the base speed, a full-wave voltage supply (without PWM) is used to obtain a wide constant-power range.

In the following, a comparative analysis of both motors for a constant-torque speed range will be carried out. Electromagnetic torque and copper losses will be expressed in relation to the dimensional parameters of the two motors. For the sake of comparison, the same calculation method as well as the same parameter notations will be used for both motors. Numerical computations will be made for a 100 Nm average torque and for fixed frame sizes of the magnetic circuit, i.e. 250 mm external diameter and 150 mm stack length.

2. Parameter analysis of DSRVM performances

The dimensional parameters of DSRVM are defined in Fig. 3. They are: N_s and N_r, the number of stator and rotor teeth (or poles), respectively; $\beta_s = \beta_s^\circ / \alpha_s^\circ$ with $\alpha_s^\circ = 2\pi / N_s$ and $\beta_r = \beta_r^\circ / \alpha_r^\circ$ with $\alpha_r^\circ = 2\pi / N_r$, the stator and rotor reduced pole arcs, respectively; R, r, the outer stator radius and the rotor radius, respectively; e, the airgap length; R_a, the shaft radius; e_c and e_{cr} the thickness of stator and rotor yoke, respectively; h_s and h_r, the stator and rotor tooth heights; L, the stack length.

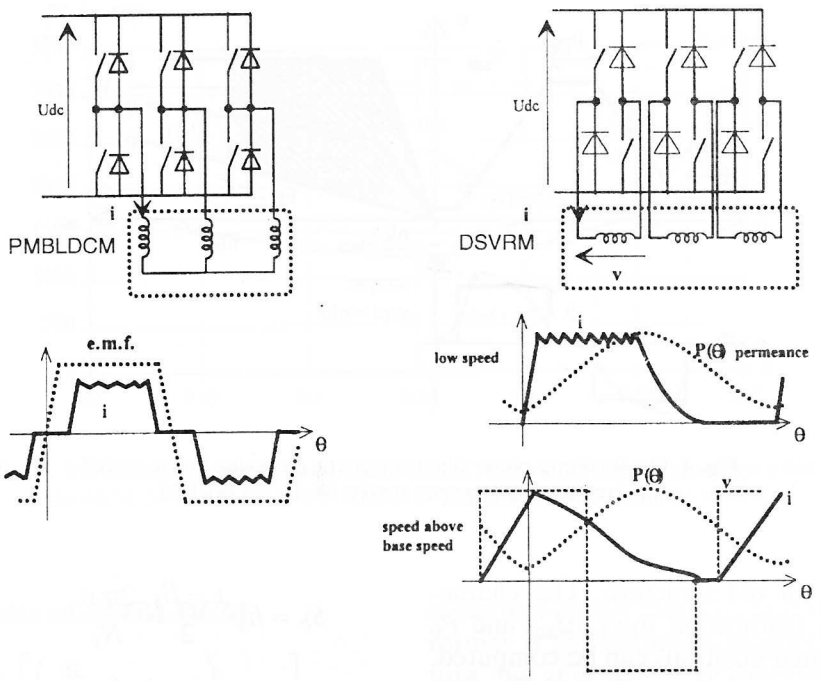

Fig. 2. Static converters and typical supply waveforms.

The basic electromagnetic characteristics of the DSVRM are defined by the flux array $\varphi(ni, \theta)$ corresponding to one phase. As a first approximation, one can suppose that there is no magnetic coupling between phases. The instantaneous torque can be computed by derivation of the coenergy W'_{em}, i.e.

$$t(\theta) = \sum_{k=1}^{q} \frac{\partial W'_{em}(nI_k, \theta_m)}{\partial \theta_m} = \sum_{k=1}^{q} N_r \frac{\partial W'_{em}(nI_k, \theta)}{\partial \theta} \quad (1)$$

with $W'_{em}(nI_0, \theta) = \int_0^{nI_0} \varphi(nI_0, \theta)\, dnI$,

where θ_m is the mechanical angle between rotor and stator, θ, the electrical angle, ni, the ampere-turns per phase and ni/p, the ampere-turns per pole.

For the sake of simplicity, it is assumed that the magnetic material has a hard saturation at B_{sat} value of the flux density; in the present case, $B_{sat} = 1.6$ T has been inferred from experiments. Fig. 4 shows in bold line the idealised form of magnetic characteristics, and in thin line their real shape. The hachured area is equal to the energy converted in one stroke for ideal supply (square ampere-turns with amplitude nI_M and angular duration $D\,\theta_p$ between unaligned positions). The average torque, which is proportional to W, yields

$$T = q\, N_r \frac{W}{2\pi} . \quad (2)$$

The idealised angles characterising the permeance waveform may be defined by rotor and stator tooth arcs [4]. It is to be noted that the angular duration of torque production is related to the stator tooth arc by

$$D\,\theta_p = N_r\, \beta_s^{\circ} . \quad (3)$$

Thus, in order to achieve a $2\pi/3$ angular duration (as required in a three-phase machine to obtain the continuity of the polyphase instantaneous torque) the reduced tooth arc β_s must be equal to or greater

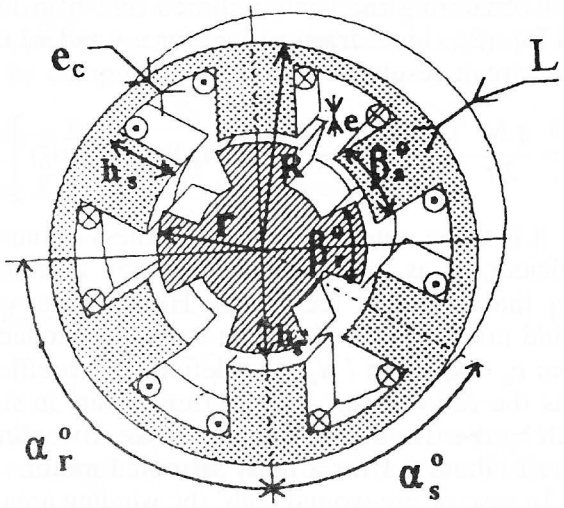

Fig. 3. DSRVM main dimensional parameters.

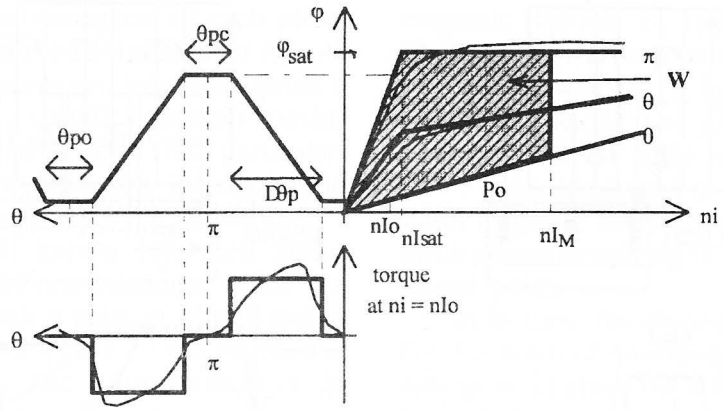

Fig. 4. Idealised one-phase electromagnetic piecewise linear model and converted energy per stroke, W, for a DSVRM.

than 0.5 in the case of 6/4 structure. The characteristic variables φ_{sat} (saturation flux), nI_{sat} and P_0 (permeance in unaligned position) can be computed, with reference to the main dimensions defined in Fig. 3, as

$$\varphi_{sat} = B_{sat} \frac{2\pi r L \beta_s}{N_s}, \tag{4}$$

$$n I_{sat} = p \frac{B_{sat}\, e}{\mu_0}, \tag{5}$$

$$P_0 = \frac{P_0^* L}{p}, \tag{6}$$

where P_0^* value is approximately 5 μH/m, if rotor tooth arc is close to the stator one. Moreover, this condition is necessary in order to obtain a wide constant-power speed range [26]. The choice of rotor pole arc is the result of a compromise between a high maximum power [15] and a low torque ripple within the constant maximum torque range.

Considering the hachured area shown in Fig. 4 and Eq. (2), the average torque for a standard magnetic circuit results as

$$T = \frac{q N_r}{2\pi} \left[\varphi_{sat}\, nI_M - \frac{1}{2} \varphi_{sat}\, nI_{sat} - \frac{1}{2} P_0\, nI_M^2 \right]. \tag{7}$$

It is to be noted that yoke thickness e_c must be sufficient, so as to achieve a saturation level lower than that of stator teeth [25]. However, its value should not cause winding area to be over-reduced. From $e_c = k_c \beta_s r \pi / N_s$, one defines the coefficient k_c as the ratio of the average flux density in stator teeth by the flux density in stator yoke. Its optimum value is about 1.1 for a fairly saturated motor.

In case of pre-wound coils, the winding area can be estimated as

$$S_b = h_s \frac{1-\beta_s}{2} \frac{2\pi r}{N_s} \approx \left[1 - k_r \left(1 + k_c \beta_s \frac{\pi}{N_s} \right) \right] \left(1 - \beta_s \right) k_r \frac{\pi}{N_s} R^2 \tag{8}$$

with $k_r = r / R$; if k_b is defined as the copper area to winding area ratio [23], for pre-wound coils it can be 0.6.

At low speeds (below the base speed) current waveform may be assumed it a quasi-square wave. A form factor

$$k_i = \frac{nI_M}{nI_{rms}}, \quad 1.5 < k_i < 1.6$$

for a three-phase motor, is introduced in order to calculate the rms ampere-turns.

Copper losses may be computed as

$$P_J = \rho \frac{2q}{p} k_l L \frac{nI_M^2}{k_i^2 k_b S_b}, \tag{9}$$

where ρ is the winding resistivity and k_l, a variable length coefficient (depending on r and β_s) taking winding ends into account. Its value is greater than unity [23].

For a required torque of 100 Nm, optimum parameter values may be determined. It appears that the airgap length has to be as narrow as possible. In present case, accounting for the overall sizes as well as the economic and environmental constraints, a minimum 0.8 mm airgap length has been found acceptable.

Fig. 5 shows the influence of k_r on copper losses at 150 °C for various values of β_s. These results were obtained for a 6/4 motor, with a 100 Nm torque, k_b, k_c and k_i being equal to 0.6, 1.1 and 1.6, respectively. Here k_r=0.57 and β_s=0.55, the latter value being consistent with the low-ripple torque requirement [24].

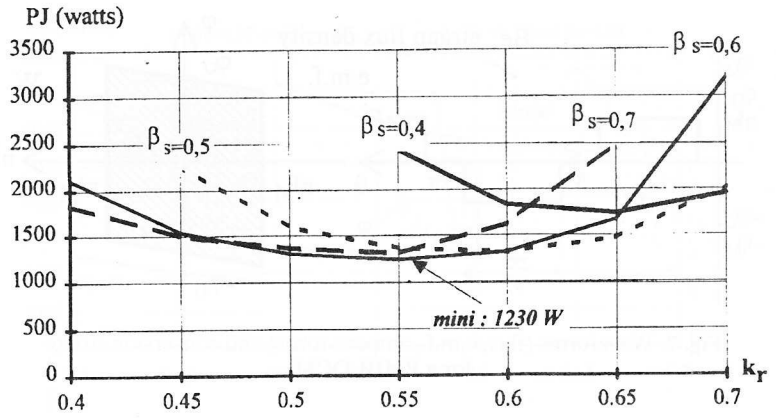

Fig. 5. Influence of airgap radius to outer radius ratio on the copper losses for a 6/4 three-phase DSRVM (T = 100 Nm, R = 125 mm, L = 150 mm, k_b = 60%).

3. Parameter analysis of PMBLDCM performances

Size parameters for PMBLDCM, which are roughly the same as for DSRVM, are defined in Fig. 6. The stator parameters are: $N_s = 2m_e pq$, the number of stator teeth, m_e being the number of slots per pole and per phase, p, the number of pole pairs and q, the number of phases; t, the tooth width, which is related to the tooth flux density, B_t; s, the slot width; i_s, the slot-opening width; e_c, the yoke thickness which is related to the flux density, B_c.

The rotor parameters are: r, the airgap radius (at magnet surface); e_a, the magnet radial thickness (magnets are contiguous); e_f, the thickness ot the non-magnetic sleeve that holds magnets; e_m, the mechanical airgap; $e = e_f + e_m$, the magnetic airgap.

Magnet characteristics were idealised and defined at a steady 150°C temperature. Their magnetization flux density B_a, relative permeability μ_{ra} and demagnetizing field H_{dem} were assumed to be constant. Two types of magnets were considered, i.e. samarium-cobalt (Sm-Co) and strontium-ferrite. The former is the strongest magnet at a given temperature, but it is also very expensive (≅ 300 Ecus/kg). Ferrite magnets themselves are the most economical ones (≅ 6 Ecus/kg) and are especially attractive for mass production. Comparative features of both magnet types, at 150 °C, are given below:

Ferrite: B_a=0.29 T, μ_{ra}=1.1, H_{dem}=300 kA/m;
Sm-Co: B_a=1 T, μ_{ra}=1.05, H_{dem}=600 kA/m.

Cheaper neodymium-iron-boron (NdFeB) magnets may be used, but they have a limited maximum operation temperature. Their performances are close to those of Sm-Co magnets, hence the conclusions drawn from this study may be entirely transposed to NdFeB magnets.

Magnets with performances between those of Sm-Co and ferrites are also available, such as bonded NdFeB [3], but their limited maximum temperature raises problems for their design of high specific power motors operating at high temperatures.

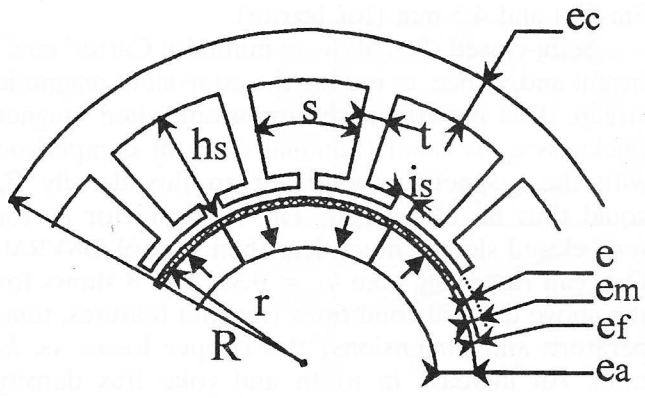

Fig. 6. Size parameters for a surface-mounted PMBLDCM.

Airgap flux density B_e remains constant under poles (if slot permeance modulation is omitted) and may be computed as

$$B_e = B_a \frac{e_a}{e_a + \mu_{ra} K_c e} K_{fa}\,, \tag{10}$$

where K_c denotes Carter's coefficient,

$$K_c = \left[1 - \frac{N_s \left(\frac{i_s}{e}\right)^2 e}{\left(5 + \frac{i_s}{e}\right) 2\pi r}\right]^{-1}, \tag{11}$$

and K_{fa} is a form factor taking into account the non-rectangular shape of surface magnets [11],

$$K_{fa} = 1 - \frac{e_a}{2r}\,. \tag{12}$$

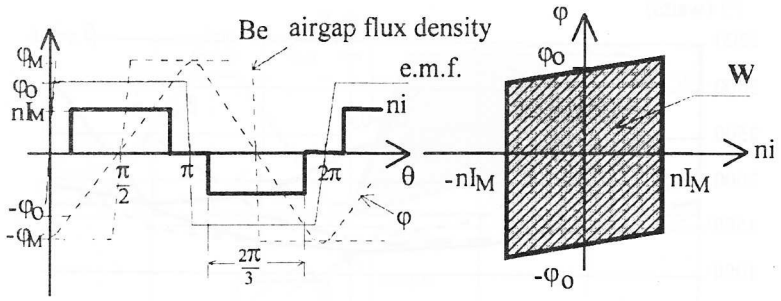

Fig. 7. Waveforms (flux, e.m.f., ampere-turns) and conversion stroke for a PMBLDCM.

Fig. 7 shows the waveforms of the airgap flux density, flux linkage for one turn, e.m.f. and feeding ampere-turns, for definite conditions (contiguous magnets, $m_e = 1$ etc.).

As the permeance is not dependent on the angular position, the PMBLDCM instantaneous torque may be written as

$$t(\theta) = \sum_{k=1}^{q} p \frac{\mathrm{d}\varphi_k}{\mathrm{d}\theta} n i_k \,. \tag{13}$$

The converted energy per stroke is

$$W = 4\,\varphi_0\, n I_M \,, \tag{14}$$

where φ_0 defines the flux value at the current commutation, i.e.

$$\varphi_0 = \frac{2}{3}\varphi_M \tag{15}$$

with $$\varphi_M = \frac{B_e \pi r L}{p} \,. \tag{16}$$

The average torque may be calculated from Eqs. (14)-(16) as

$$T = \frac{4}{3} q\, B_e\, r\, L\, n\, I_M \,. \tag{17}$$

Copper losses can be determined by using the same method as for DSRVM coefficients, k_i, k_b and k_l keeping their definitions. The value of k_i is roughly $\sqrt{3/2}$ in the case of current waveforms as shown in Fig. 7.

Yoke thickness may be computed by

$$e_c = \frac{\pi r}{2p} \frac{B_e}{B_c} \,, \tag{18}$$

where B_c (equal to 1.6 T) defines the constraint of maximum flux density.

By limiting the tooth flux density to B_t (equal to 1.8 T), the stator tooth-width results as

$$t = \frac{\pi r}{p\, q\, m_e} \frac{B_e}{B_t} \,, \tag{19}$$

the slot width as

$$s = \frac{\pi r}{p\, q\, m_e} \left[1 - \frac{B_e}{B_t}\right] \tag{20}$$

and tooth height as

$$h_s = R - r - e_c - e \,. \tag{21}$$

The copper losses can be expressed by the formula

$$P_J = \rho \frac{2q}{p} k_l L \frac{n I_M^2}{k_i^2 k_b m_e S_b} \,, \tag{22}$$

which is similar to Eq. (9). One can analyse the influence of several parameters on copper losses for a given torque. Magnet thickness e_a has to be determined first. It has to be great enough, so as to avoid demagnetization at maximum current [13], but also small as possible, so as to reduce the magnet cost. When optimizing dimensional parameters, e_a must be maintained above demagnetization threshold. For Sm-Co and ferrite, e_a has obtained the values of 3 mm and 20 mm, respectively.

To stand a maximum speed of 12 000 rpm with a 150 mm rotor diameter, polyglass sleeves were adopted, the thickness, e_f, of which was of 1.5 mm (for Sm-Co) and 3 mm (for ferrite). The value of mechanical airgap e_m being less crucial than for DSVRM, it was designed with a 1.5 mm length. Hence, magnetic airgap e has resulted of 3 mm (for Sm-Co) and 4.5 mm (for ferrite).

Semi-closed slots allow to minimise Carter' coefficient and, hence, to reduce the equivalent magnetic airgap. This is particularly important when magnet thickness e_a is small (minimal cost) in comparison with the magnetic airgap. Airgap flux density B_e could thus be maximized. The filling factor k_b for semi-closed slots is much less than that of DSVRM. One can resonably take $k_b = 0.35$. Fig. 8 shows for the above defined conditions (magnet features, temperature and dimensions) the copper losses vs. k_r ratio. An increase in tooth and yoke flux density would enable greater winding area and reduced copper losses, while higher iron losses would results. As

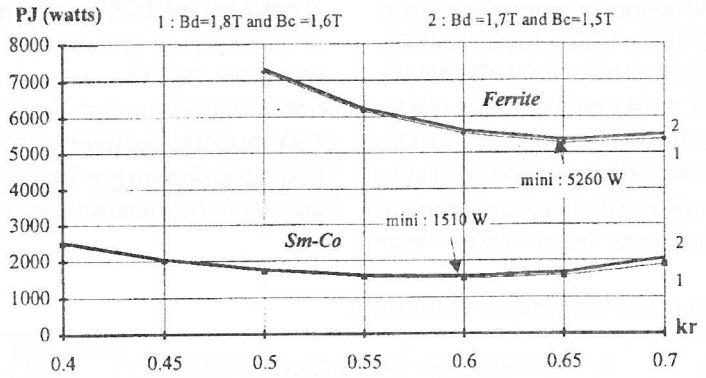

Fig. 8. Influence of airgap radius to outer radius ratio on the copper losses for a four-pole PMBLDCM (T=100 Nm, R=125 mm, L=150 mm, k_b=35%).

could be seen, ferrite motor shows copper losses much higher than Sm-Co motor (3.5 ratio).

Carter's coefficients K_c are 1.23 and 1.26, and the average airgap flux densities B_e yield 0.43 T and 0.194 T for Sm-Co and ferrite motors, respectively.

For Sm-Co PMBLDCM whose magnet thickness was not very great as against magnetic airgap length, the airgap flux density was weak. A 4 mm magnet thickness instead of 3 mm would cause copper losses to decrease from 1510 W to 1260 W, i.e. a 17% reduction. Moreover, magnet weight would shift from 1.72 to 2.28 kg and magnet cost would roughly rise from 500 to 650 Ecus. As a comparison, 20 mm-thick ferrite magnets have a 6.7 kg weight and their cost is about 40 Ecus.

The increase in the number of pole pairs would allow a substantial decrease in copper losses. Thus, with 4 pairs of poles instead of 2 for the Sm-Co and ferrite PMBLDCM, copper losses decrease from 1510 to 790 W, and from 5260 to 3100 W, respectively. This is achieved mainly due to the shorter turn-ends, which means that k_l decreases.

4. Performance comparison of DSVRM and PMBLDCM

The parameter analysis of both DSVRM and PMBLDCM carried out above was focused on the average torque and copper losses. Both types of motors displayed comparable characteristics. Eqs. (9) and (22) show that copper losses are proportional to k_l coefficient. Therefore, when there are few poles, DSVRM gives better results than PMBLDCM due to its concentrated coils. For optimal parameters of the motors, k_l values were 1.6, 2.45, and 2.62, for DSVRM, Sm-Co and ferrite PMBLDCM, respectively.

A comparison of copper losses as a function of magnetic airgap for the three motors is given in Fig. 9. For the two PMBLDCM copper losses curves are depicted by dotted lines when magnetic airgap becomes smaller than the sleeve thickness required for maximum speed. One can note that copper losses are smaller for Sm-Co motor than for DSVRM, for the same airgap value, and that ferrite motor gives

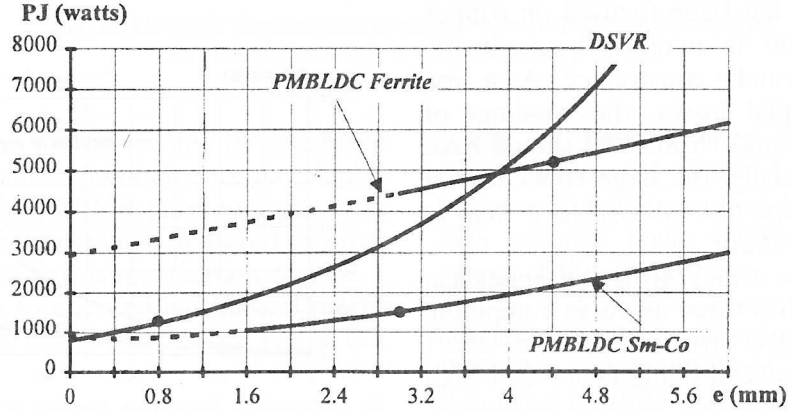

Fig. 9. Comparison of copper losses as a function of magnetic airgap for DSVR and PMBLDC motors.

better results than DSVRM when magnetic airgap is greater than 4 mm. For the same filling factor (60%), copper losses have been 1240, 880 and 3070 W for DSVRM, Sm-Co and ferrite PMBLDCM, respectively.

The main features of the three motors, at the first level of optimization, are summarized in Table 1. Their airgap length constraints, i.e. mechanical limit or sleeve thickness, have been taken into account (magnetic airgap: 0.8 mm for DSVRM, respectively, 3 mm and 4.5 mm for Sm-Co and ferrite PMBLDCM). The average torque was 100 Nm, the outer diameter and the stack length were 250 and 150 mm, respectively. In Table 1, A_L denotes the magnetic loading (A/m), δ, the rms current density and σ_T, the magnetic airgap shear stress.

Table 1. Comparative main features of DSRVM and PMBLDCM.

	k_i	k_b	k_l	nI_M (A)	A_L (kA/m)	δ (A/mm^2)	B_e (T)	P_J (W)	σ_T (N/cm^2)
DSVRM	1.6	0.6	1.6	6940	60.2	7.9	–	1240	2.24
Sm-Co PMBLDCM	1.225	0.35	2.45	5180	53.8	6.5	0.429	1510	1.89
ferrite PMBLDCM	1.225	0.35	2.62	10574	101.5	10.3	0.194	5260	1.6

For DSVRM, inertia is lower for two reasons. First because optimization leads to a smaller airgap radius, second because the rotor has a toothed structure which reduces by more than half the inertial volume (β_r<0.5); but this parameter is of little importance in the case of an electric vehicle.

Table 2 summarizes the influence of the number of poles (N_s / N_r, for DSVRM, and number of pole pairs p, for PMBLDCM) on the copper losses for both motor types. An increase of number of poles is more advantageous for PMBLDCM whose full-pitch winding turn-ends are considerably shortened. Such a shortening is less advantageous for DSVRM due to its concentrated coils. Besides, the 6/8 structure for DSRVM has very good perfomances, i.e. copper losses are half as for 6/4 DSRVM.

Table 2. Comparison of copper losses for DSVRM and PMBLDCM.

DSVRM	P_J (W)	PMBLDCM	P_J (W) Sm-Co	P_J (W) ferrite
6/4	1240	2p=4	1510	5260
6/8	600	2p=6	1010	3780
12/8	990	2p=8	790	3080

The evolution of copper losses vs. average torque is shown in Fig. 10 for the three investigated motors.

Though this study has been focused on copper losses, one should bear in mind that an electric machine is mainly thermally constrained. As a first approximation, for equal losses, the windings of similarly sized DSVRM and PMBLDCM should have the same heating. Actually, the large concentrated windings of DSVRM are not favourable if heat is exchanged outside the stator.

Briefly, even if the DSRV structure appears a priori less efficient, it has three assets in competing with rare-earth PMBLDC structures, i.e. its short winding turn ends, good coil-filling factor and high saturation flux density.

Concerning PMBLDCM, a flux concentrating arrangement of the magnets [14] would greatly improve the airgap flux density, particularly in the case of ferrite motors; however such a rotor would required a great number of pole pairs (6 to 8).

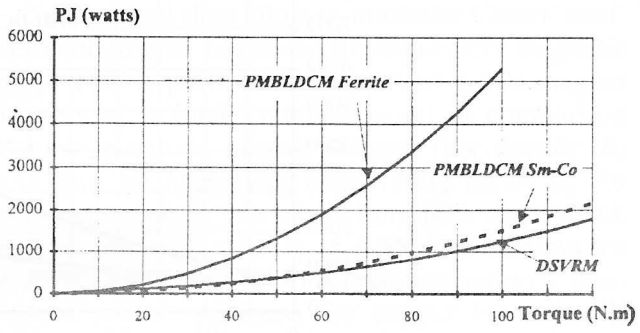

Fig. 10. Copper losses vs. average torque for DSVRM and PMBLDCM.

5. Experimental results for a 27 kW DSVRM

It has been designed and built a 6/4 DSVRM as an electric vehicle drive. The required performances were 100 Nm and 27 kW in the speed range of 2500 to 10 000 rpm. The main experimental results [26] are given below.

The converter comprises three asymmetrical half bridges with 400 A IGBT under 120 V DC supply. Each phase consists of 23 turns (9 parallel strands with 1.9 mm diameter). The main dimensions of the motor are: L=150 mm, R=125 mm, r=75 mm, h_s=25.6 mm, h_r=28 mm, e=0.8 mm and e_c=23.6 mm.

Fig. 11 shows flux and torque characteristics measured on the prototype DSVRM.

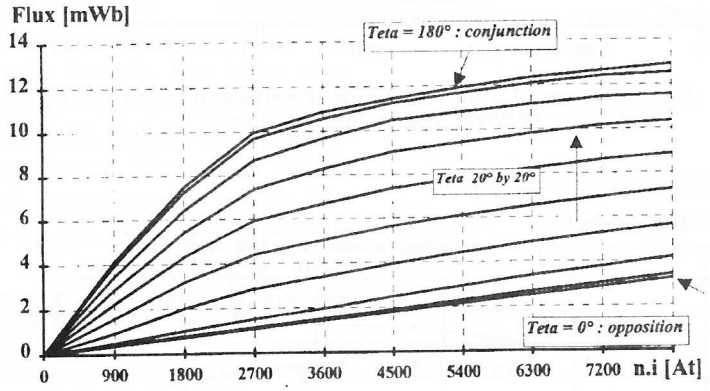

(a)

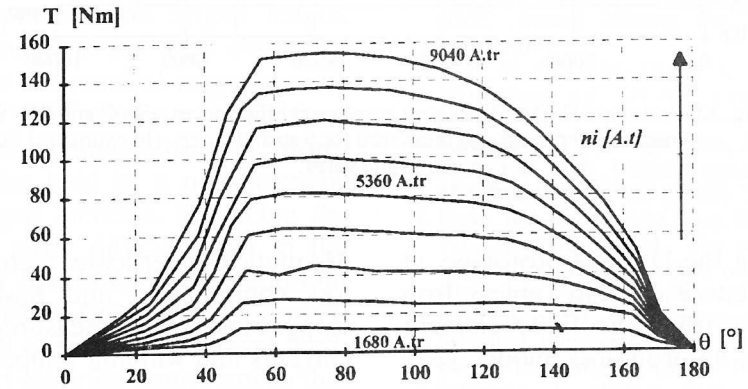

(b)

Fig. 11. DSVRM characteristics of magnetic flux **(a)** and static torque **(b)** as a function of phase ampere-turns and position.

At low speeds, the motor was fed by optimized current waveforms so as to minimize torque ripples [18, 24]. At high speeds, 27 kW maximum power in the 2500 to 10 000 rpm range was achieved through the control of advance and magnetization angles.

Fig. 12 shows the torque and mechanical power available with the IGBT converter under 120 V DC supply.

DSVRM efficiency curves without converter at 27 kW maximum power are depicted in Fig. 13. One curve represents measured efficiency at maximum power for 9 strand wires; at 10 000 rpm, magnetic copper losses (of almost 1.9 kW) were dissipated because of the important leakage field due to the high advance angle required to reach maximum power at this speed.

The other curve shows the estimated enhanced efficiency for 36 strand wires of 0.95 mm diameter. With this simple solution, magnetic copper losses should be fourfold reduced; at 10 000 rpm, windage losses reach 600 W mainly due to the rotor saliency.

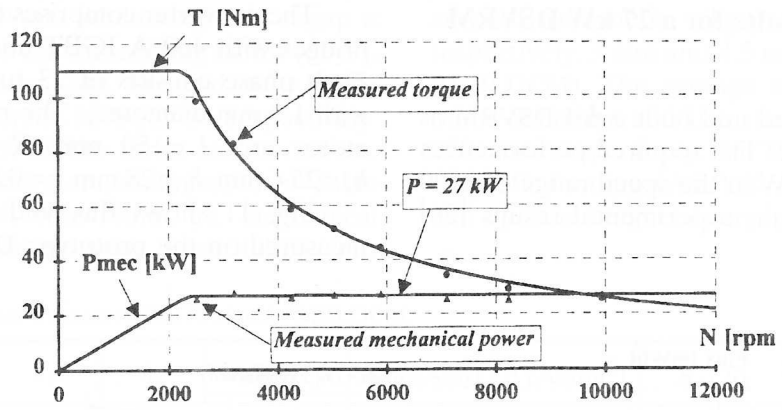

Fig. 12. Maximum power and torque available with the prototype DSRVM under 120 V DC supply.

Fig. 13. Prototype DSRVM (without converter) efficiency at 150°C and 27 kW mechanical power; **(a)** measured for 9 strand wires; **(b)** estimated for 36 strand wires.

Losses distribution in the DSVRM prototype, at 2500 and 10 000 rpm speeds, is given in Table 3. Iron losses were computed by using the finite element method associated with an iron loss model [25]. Magnetic copper losses were estimated through iron loss computation and power loss measurements. Copper losses were measured knowing the rms phase currents and winding temperature.

Table 3. Prototype DSRVM losses distribution at 27 kW mechanical power.

motor speed	copper losses	iron losses (estimated)	magnetic copper losses (estimated)	windage losses
2 500 rpm	1100 W	450 W	—	—
10 000 rpm	900 W	220 W	1900 W	600 W

6. Conclusions

In this paper, the average torque and low-speed copper losses of DSVRM and PMBLDCM were computed via simplified electromagnetic models. Economical ferrites and high-performance rare-earth magnets were selected. The resluts have been applied to a single-motor urban electric vehicle, the motor characteristics being (i) 100 Nm torque in the 0 to 2500 rpm range, (ii) 27 kW maximum power in the 2500 to 10 000 rpm range and (iii) 12 000 rpm overspeed. Frame size constraints have been imposed.

In the case of PMBLDCM, magnet thickness is determined by the demagnetization limit at maximum torque. Moreover, to hold magnets at high speeds a sleeve is required, which in turn determines the magnetic airgap length.

In the case of DSVRM, the airgap length has been minimized, while keeping in mind the constraints specific to electric vehicles. Owing to the relatively high maximum speed, the electric frequency has been limited by selecting a 6/4 DSVRM and a four-pole PMBLDCM, respectively.

The influence of several parameters, such as the airgap radius and magnetic length, has been emphasized. The comparison showed that DSVRM has smaller copper losses due to its short winding turn-ends and good coil-filling factor. The effect of increasing the pole number upon copper losses has been also assessed; with 4 pairs of poles, rare-earth PMBLDCM proves to be more efficient than DSVRM. Ferrite PMBLDCM performances are far inferior to those of DSVRM.

To conclude, the advantages and drawbacks of each motor type can be summarized as follows:

- Due to its simple excitation, PMBLDCM has low copper losses, especially at low torques, provided that magnets are sufficiently strong. Besides, its characteristics are little dependent on airgap length. However, high-energy magnets are very expensive for mass production, and economical magnets, such as ferrites, yield poor performances. Maximum torque is limited by magnet demagnetization. Moreover, magnets have to be held by a non-magnetic sleeve which causes airgap increase. Balancing the heterogeneous rotor is more difficult than in the case of DSVRM. When operating in the constant maximum-power range, PMBLDCM requires buried-magnet rotor [19] as well as sinusoidal current feeding; converter rating then becomes equivalent to that of DSVRM.

- DSVRM certainly is the most economical electric motor suitable for automatic production. Its feeding converter is both simple and safe thanks to its asymmetrical half-bridge structure as well as its electrically and magnetically independent phases [20]. The performances of this motor are relatively dependent on magnetic airgap length, which has to be sufficiently low in order to keep copper losses below the level of those of rare-earth PMBLDCM. However, the torque ripple is high. At low speeds, this problem is solved by optimizing current control [18], but at high speeds the problem remains. Moreover, owing to its structure and principle of electromechanical conversion, this type of motor is noisier than its competitors [21]; it still has to be improved so as to meet electric vehicle requirements.

- The comparison has shown that DSVRM is a valuable solution for electric vehicle drives, although, for the moment, research efforts aim at induction and synchronous motor types [22].

- The 6/4 DSVRM, that has been designed and built, complies with the following schedule of conditions: 100 Nm and 27 kW in the 2500 to 10 000 rpm range. It has been demonstrated that the 6/4 DSVRM is able to convert a torque with low ripple at low speeds, on the one hand, and to run at maximum power within a wide speed range, on the other hand.

Acknowledgement

The authors would like to thank the AUXILEC Electric Vehicle Department for building the DSVRM prototype and providing the testing bench.

References

1. Miller, T.J.E., *Brushless permanent-magnet and reluctance motor drives*. Oxford, Oxford Science Publications, 1989.
2. Laurent, P., Gabsi, M., Multon, B., Sensorless rotor position analysis using resonant method for switched reluctance motor. *IEEE Annual Meeting Ind. Appl. Soc.*, Toronto, 1993, pp. 687-694.
3. Jufer, M., Crivii, M., Hatefi, K., Switched synchronous motors. *Proceedings of SM-100 Conf.*, Zürich, Part II, 1991, pp. 455-459.
4. Lawrenson, P.J., Stephenson, J.M., Blenkinsop, P.T., Corda, J., Fulton, N.N., Variable-speed switched reluctance motors. *IEE Proc. - Pt. B*, 127 (1980), 253-265.
5. Blake, R.J., Davis, R.M., Ray, R.M., Fulton, N.N., Lawrenson, P.J., Stephenson, J.M., The control of switched reluctance motors for battery electric road vehicles. *IEE Conf. Power Electr. and Var. Speed Drives*, London, 1984, pp. 361-364.
6. Lawrenson, P.J., Stephenson, J.M., Fulton, N.N., Corda, J., Switched reluctance motors for traction drives. *Proc. Int. Conf. Electr. Mach.*, Athens, 1980, pp. 410-417.
7. Sebastian, T., Slemon, G.R., Operating limits of inverter-driven permanent magnet motor drives. *IEEE Trans. Ind. Appl.*, 23 (1987), 327-333.
8. Jufer, M., *Transducteurs électromécaniques*, Lausanne, Presses Polytechniques Romandes, 1985.
9. Schifferl, R.F., Lipo, T.A., Power capability of salient pole permanent magnet synchronous motors in variable speed drive applications. *IEEE Trans. Ind. Appl.*, 26 (1990), 115-123.
10. Tormey, D.P., Torrey, D.A., Levin, P.L., Minimum airgap-permeance data for the doubly-slotted pole structures common in variable-reluctance motors. *IEEE Annual Meeting Ind. Appl. Soc.*, Seattle, 1990, pp. 196-200.
11. Boules, N., Two-dimensional field analysis of cylindrical machines with permanent magnet excitation. *IEEE Trans. Ind. Appl.*, 20 (1984), 1267-1277
12. Jacques, C., Moteur synchrone autopiloté à fort couple et haute compacité. *Journées DRET Electrotechnique Avancée*, 1989, 13 pp.
13. Demerdash, N.A., Miller, R.H., Nehl, T.W., Overton, B.P., Ford, C.J., Comparison between features and performance characteristics of fifteen H.P. samarium cobalt and ferrite based brushless DC motors operated by the same power conditioner. *IEEE Trans. Power App. Syst.*, 102 (1983), 104-112.

14. Labraga, M., Davat, B., Lajoie-Mazenc, M., Conception d'un servomoteur à aimants permanents ferrites à entraînement direct. *Compte-rendu 5e Colloque sur les Moteurs Pas à Pas*, Nancy, 1988, pp. 125-134.
15. Multon, B., Hassine, S., Le Chenadec, J.Y., Pole arcs optimization of vernier reluctance motors supplied with square-wave current. *Electric Machines and Power Systems*, 21 (1993), 695-709.
16. Multon, B., Glaize, C., Optimisation du dimensionnement des alimentations des machines à réluctance variable. *Revue de physique appliquée*, 22 (1987), 339-357.
17. Multon, B., Glaize, C., Size power ratio optimization for the converters of switched reluctance motors. *Proc. IMACS TC1 '90*, Nancy, 1990, pp. 325-331.
18. Le Chenadec, J.Y., Multon, B., Hassine, S., Current feeding of switched reluctance motor. Optimization of the current waveform to minimize the torque ripple. *Proc. IMACS TC1 '93*, Montreal, 1993, pp. 267-272.
19. Jahns, T.M., Kliman, G.B., Neumann, T.W., Interior permanent-magnet synchronous motors for adjustable-speed drives. *IEEE Trans. Ind. Appl.*, 22 (1986), 738-747.
20. Stephens, Ch.M., Faulty detection and management system for fault-tolerant switched reluctance motor drives. *IEEE Trans. Ind. Appl.*, 27 (1991), 1098-1102.
21. Cameron, D.E., Lang, J.H., Umans, S.D., The origin and reduction of acoustic noise in doubly-salient variable-reluctance motors. *IEEE Trans. Ind. Appl.*, 28 (1992), 1250-1255.
22. Riezenman, M.J., Electric vehicles (special report). *IEEE Spectrum*, 1992, 18-24, 93-101.
23. Multon, B., Jacques, C., Comparaison de deux moteurs électriques autopilotés: le moteur synchrone à aimants permanents et le moteur à réluctance variable à double saillance. *Compte-rendu Symp. Véhicules Propres-Réalités et Perspectives du Véhicule Electrique*, La Rochelle, 1993, pp. 295-302.
24. Le Chenadec, J.Y., Geoffroy, M., Multon, B., Mouchoux, J.C., Torque ripple minimisation in switched reluctance motors by optimisation of current waveforms and teeth shape with copper losses and V.A. silicon constraints. *Proc. Int. Conf. Electr. Mach.*, Paris, 1994, vol. 3, pp. 559-564.
25. Hoang, E., Multon, B., Vives-Fos, R., Geoffroy, M., Influence of stator yoke thickness and stator teeth shape upon ripple and average torque of switched reluctance motors. *Proc. Symp. Power Electronics, Electrical Drives and Advanced Motors* , Taormina, 1994, pp. 145-149.

Received January 31, 1995

Assoc. Prof. Bernard Multon

Ing. Emmanuel Hoang

Ing. François Camus

Laboratoire d'Électricité, Signaux et Robotique (LÉSiR)
École Normale Supérieure de Cachan
61, Avenue du Président Wilson
F - 94235 Cachan Cédex, France